Corrosion performance of electroless Ni-B coatings reinforced with YSZ nanoparticle

C.Chenna Raidu[a,b], N. Arunachalam [b,*] and S. Boominatha sellarajan [b]

[a]*Combat Vehicles Research & Development Establishment (CVRDE), DRDO, Chennai–600054, India*

[b] *Department of Mechanical Engineering, Indian Institute of Technology Madras, Chennai–600036, India*

**Corresponding Author Email: chalam@iitm.ac.in*

Abstract :

This study investigates the corrosion performance of an electroless coating incorporating 3 mol% YSZ nanoparticle reinforcement in the matrix of Ni-B. The objective is to produce a nanoceramic composite coating and analyze its impact on corrosion properties in both untreated and treated conditions. The composition of the coatings is identified using energy-dispersive X-ray (EDX) spectroscopy and particle dispersion and coating thickness are investigated using scanning electron microscopy (SEM). Further, hardness is evaluated through Vickers micro hardness tests and structural analysis by X-ray diffraction (XRD). Potentiodynamic polarization provides insights into the corrosion resistance or susceptibility of the material. At the same time, electrochemical impedance spectroscopy (EIS) evaluates the electrochemical properties of a system or material over a broader frequency range (10 mHz-1 MHz). The findings indicate that the heat-treated coatings exhibit high hardness due to strengthening mechanisms associated with the crystalline structure, but it also results in a decrease in corrosion resistance. Specifically, in the case of the Ni-B alloy, the heat-treated (HT) coatings display lower corrosion resistance compared to the as-plated Ni-B coatings. Conversely, in the case of heat-treated Ni-B-YSZ coatings, the corrosion resistance exceeds that of the as-plated nano-composite coatings. These findings reveal potential applications of YSZ-reinforced Ni-B coatings for combating environments prone to corrosion and thus demonstrating enhanced strength for numerous versatile fields of application.

Keywords: *Electroless, Nickel Boron, Corrosion, EIS, Ni-B-YSZ.*

1. Introduction

The behaviour of coatings in harsh environments has a significant impact on the reliability and durability of components in industries such as automotive, aerospace, gas turbine and marine [1,2]. Electroless nanocomposite coatings offer a promising solution by providing uniform coating thickness and strong adhesion to complex shapes [3]. These coatings typically contain a high boron content of approx. 6-8%, which can contribute to increased hardness. Heat treatment can lead to further improvement in the hardness of the material [4]. This improvement is attributed to changes in its crystalline structure, which promotes the formation of nickel borides (Ni_2B and Ni_3B). This transition enhances wear resistance but may deteriorate the corrosion resistance of the coating due to its heterogeneous composition that can induce galvanic coupling [5]. In addition to that, Ni-B alloy coatings are less corrosion-resistant than Ni-P variant [6]. To address this, YSZ (Yttria-Stabilized Zirconia) ceramic nanoparticles are incorporated into the Ni-B matrix to form nanocomposites. These nanocomposites possess unique properties, such as excellent thermal insulation, high wear resistance and resistance to corrosive environments, making them suitable for various applications across different industries. However, despite their potential, the behaviour and corrosion protection of YSZ coatings within the Ni-B matrix, particularly under heat-treated conditions, have not been extensively investigated.

This research investigates the corrosion resistant properties of YSZ-reinforced Ni-B matrix in untreated and treated conditions. In order to accomplish this, the study utilized various characterization techniques to analyze the

coatings' surface morphology, structural features, microhardness, and electrochemical properties. This comprehensive evaluation provides valuable insights into their performance and resistance to corrosion, facilitating their suitability for diverse applications.

2. Materials and Methods

In this study, a coating was applied to high-strength low alloy steel (AISI 4140) using the well-known electroless coating. The steel samples were 20 x 20 x 4 mm3 in size and were first prepared by grinding and polishing with 800 and 1200 grit abrasive papers. Consequently, after acetone cleaning for 10 minutes at 55°C in an ultrasonic bath, the surface was pickled in a 50% HCl solution for one minute and rinsed with de-ionized water before being coating [7].

An electroless coating bath was prepared as per the given Table 1 [8,9]. In addition to the Ni-B alloy, the YSZ particles were plated by electroless method using an alkaline borohydride-reduced type-2 coating process in accordance with ASTM B607-91 (2003) [10], The YSZ nano-suspensions were prepared separately with sodium dodecyl sulphate (SDS) using ultrasonic agitation process [11]. The prepared nano-suspension (1 g/L) was added to the plating solution after 15 minutes of initial Ni-B coating to improve particle adherence and dispersion in the Ni-B matrix [12]. The coating process was done in a 200 mL bath with a pH of 13.5 and the temperature of 95±1 °C.

Table 1. Electrolyte bath composition

Chemical	Formula	g/L
Nickel Chloride hexahydrate	$NiCl_2$ $6H_2O$	20.0
Sodium Borohydride	$NaBH_4$	01.0
Ethylenediamine	$C_2H_8N_2$	59.0
Sodium Hydroxide	NaOH	40.0
Lead Nitrate	Pb $(NO_3)_2$	0.015
Sodium dodecyl sulfate	$CH_3(CH_2)_{11}OSO_3Na$	0.025
Yttria stabilized zirconia (30-80 nm)	3 mol % Y_2O_3-ZrO_2--	1.0

A baffle furnace was used to heat-treat the coated samples. The heating technique entailed increasing the temperature from ambient to 400 °C and soaking it for an hour. Subsequently, the samples were cooled inside the furnace until they reach room temperature. This heat treatment method is widely used and has been optimized by many researchers for such coatings [4,13]. Scanning electron microscopy (SEM, FEI) was used to analyze the surface morphology of coatings. An X-ray diffractometer (XRD) with Cu-Kα radiation was used to ascertain structural properties. Microhardness testing was conducted on the coatings using a Matsuzawa MMT-X7 model with a Vicker's diamond indenter, by ASTM standards E92-03 [14] and E384. Hardness measurements were performed at multiple locations, and the analysis considered the average of five different locations for the evaluation. The corrosion test of both, polarization tests in accordance with ASTM G5-14 [15] and electrochemical impedance tests in accordance with ASTM G106-10 [16] were carried out in a 3.5% NaCl solution at ambient temperature using an AMETEK multichannel potentiostat with a three-electrode configuration, the experiment scans between -0.25 and 0.25 V vs. open circuit potential at a rate of 1 mV/s using graphite as the counter electrode and a standard calomel electrode (SCE) as the reference electrode.

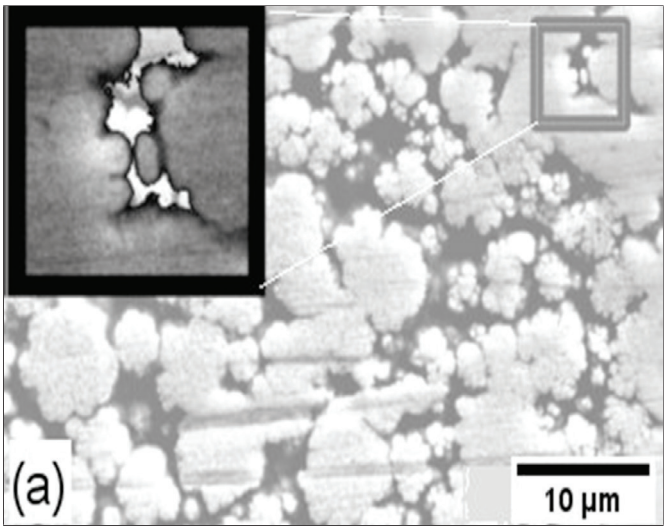
3. Results and Discussion

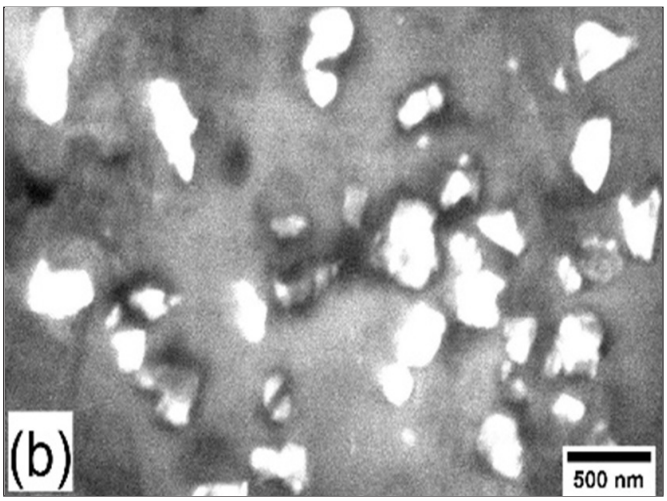
3.1 Microstructural characteristics

Figure 1a illustrates the surface morphology of Ni-B-YSZ coating which shows a distinctive broccoli-like structure characterized by smaller and finer nodules than Ni-B alloy coatings [17]. The inset of Fig 1a with enlarged image highlights the embedded particles which hinder the grain flow. The particles dispersion of YSZ in the Ni-B matrix is shown in Fig.1b. The plating process efficiently incorporates particles into the coating without much agglomeration. Particle dispersion in the coating plays a crucial role in enhancing its hardness, wear resistance, and corrosion resistance [18]. The particles act as barriers, impeding the movement of corrosive species and restricting their access to the substrate [11]. This dispersion is essential

for achieving improved protective properties in the coating. As a result, the corrosion process is decelerated, ensuring long-term protection against corrosion [19].

Figure 1c depicts a cross-sectional image of Ni-B-YSZ, HT coating with typical thickness of ~18 ± 1 µm, which is within the usual range of electroless coating deposition rates [17]. The coating looked uniform and was devoid of pin holes, voids, or agglomeration, emphasizing its strength. Heat treatment strengthens the coating further, potentially sealing pores. This results in higher impedance across a broad frequency spectrum indicating enhanced corrosion resistance. Further, the white layer is absorbed at the coating-substrate interface as a result of chemical reactions or phase transformations. This white layer serves as an additional barrier layer, offering supplementary protection against corrosion, wear and environmental factors.





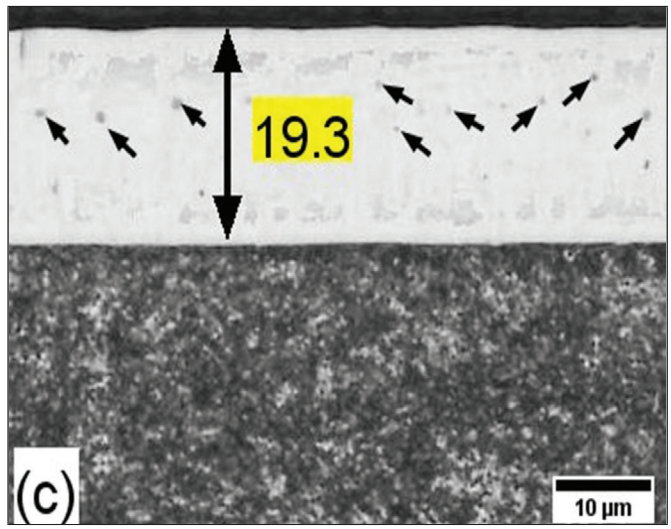


Fig 1. SEM images of (a) Ni-B-YSZ surface and its (b) dispersion and (c) cross section

The XRD analysis of the Ni-B coating, illustrated in Fig. 2a, reveals its amorphous nature in the untreated condition [20]. It exhibits a single broad peak corresponding to (111) at 2θ ≈ 43.64° plane of FCC nickel. During heat-treatment, electroless Ni-B coating undergoes a transformation and the nickel (Ni) and boron (B) atoms rearrange and react with each other to form Ni2B and Ni3B solid solutions. This transformation occurs as a result of diffusion and interatomic bonding at elevated temperatures, leading to the formation of new crystalline phases within the coating structure. The crystalline phases are identified as Ni2B (211) at 2θ ≈ 45.24° and Ni3B (201) at 2θ ≈ 46.32°. These compounds are harder than the base alloy matrix, resulting in improved wear resistance and mechanical properties [21,22].

Figure 2b illustrates the phase orientation and structural characteristics of heat treated Ni-B-YSZ coatings. The analysis reveals the presence of several peaks, with notable peaks observed at 2θ ≈ 45.78° corresponding to the NiY (131) phase and at 2θ ≈ 46.89° corresponding to the YSZ (222) phase.

These peaks provide clear identification of the YSZ material within the coating. The sharp and well-defined nature of these peaks indicates a high degree of crystallinity in the heat-treated coatings [23].

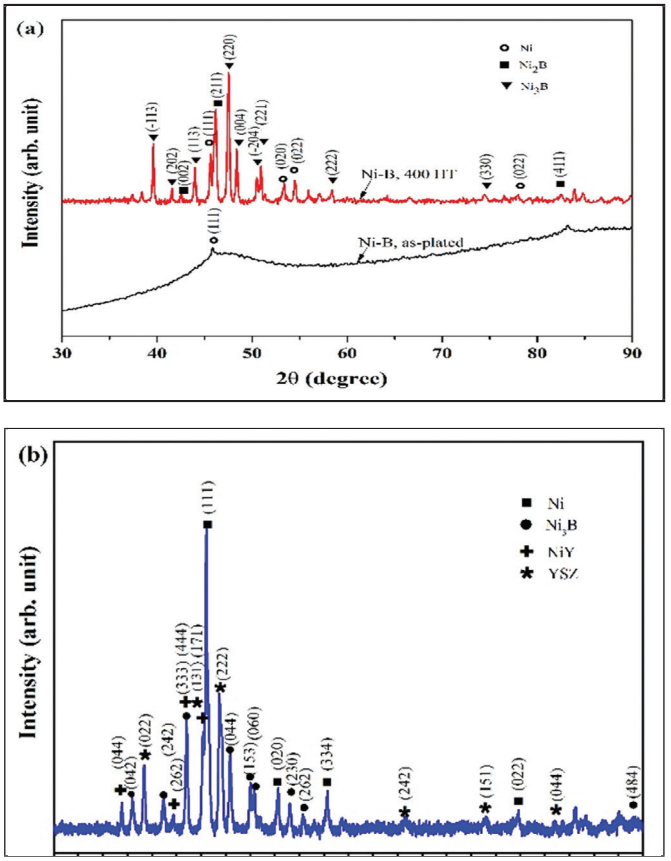
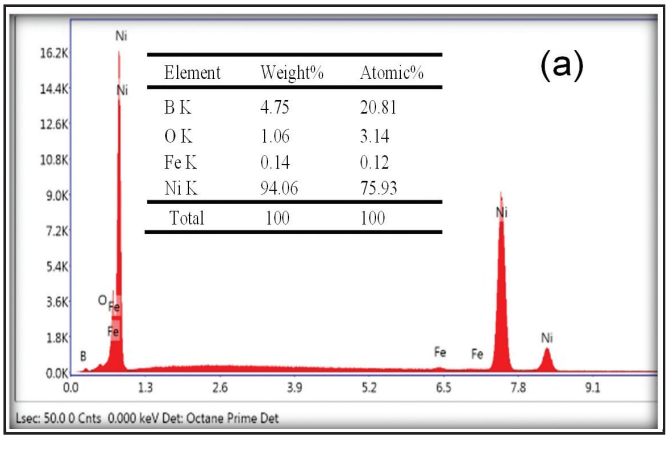


Fig. 2. XRD spectra of (a) Ni-B alloy coatings un-treated and treated condition and (b) heat treated Ni-B-YSZ.

Figure 3a shows the EDX spectra containing 6-8% of nickel and boron elements. The content of boron is an influential factor for the mechanical and corrosion properties of the coating. In the case of Ni-B-YSZ electroless coating (Fig 3b), the EDX analysis reveals the presence of Y and Zr elements, providing information about their distribution within the coating. Additionally, any potential impurities or undesired elements that could influence the coating's performance can be identified through this analysis.



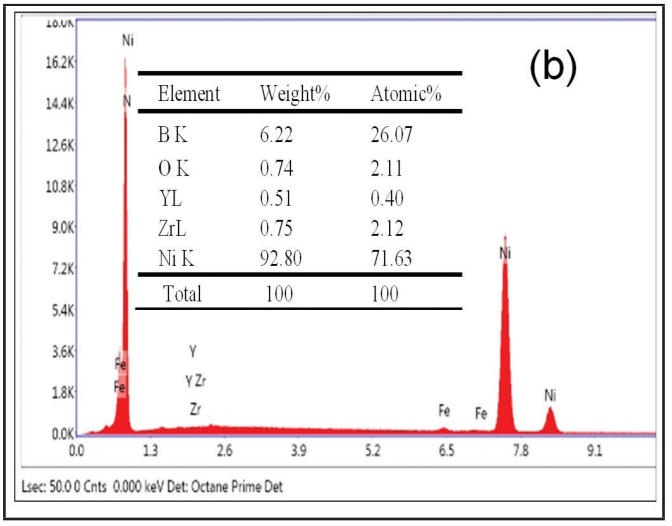


Fig. 3. The EDX elemental composition includes coatings made of (a) Ni-B alloy and (b) Ni-B-YSZ composite.

Vickers` microhardness is employed to assess hardness of the coatings. Upon heat treatment, the untreated Ni-B coating exhibits an increase in hardness from 806 ± 10 HV0.1 to 1080 ± 14 HV0.1. In comparison, the substrate exhibits a hardness of 364 ± 12 HV0.1. The transition from amorphous to crystalline phases during the annealing process is responsible for the noticeable improvement in hardness of the coating. Additionally, the structural arrangement of tetragonal boron within the coating contributes to the enhanced hardness [24-26].

The untreated Ni-B-YSZ coating exhibits a hardness value of 980 ± 12 HV0.1, which increases to 1265 ± 16 HV0.1 after undergoing heat treatment. It is primarily due to the Orowan dispersion strengthening process. In this mechanism, the dispersed particles within the coating serve as obstacles, impeding the movement of dislocations and offering additional resistance. Several factors, including the distance between dispersed particles, the ability of hard particles to prevent dislocation motion, and the influence of grain refinement, contribute to the overall strengthening effect [11].

3.2 Corrosion properties

Figure 4a demonstrates the Tafel extrapolation curve, providing insights into the mixed anodic and cathodic reaction. The corrosion potential (Ecorr)

and logarithm of current density (icorr) were obtained by extrapolating the data from the cathodic and anodic branches of the polarization curves (βc and βa, respectively). Additionally, the polarization resistance (Rp) was calculated using the Stern-Geary equation, as described in Eq. (1) [27]. The resulting values are summarized in Table 2.

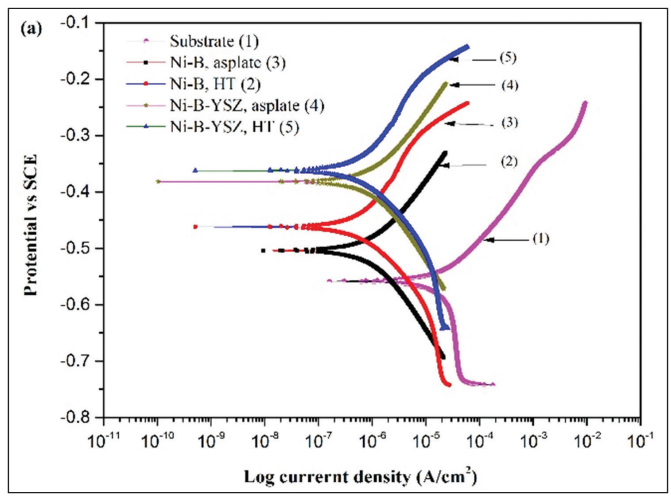
$$R_p = \frac{\beta_a * \beta_c}{2.303 * i_{corr} * (\beta_a + \beta_c)} \quad \text{-------- (1)}$$

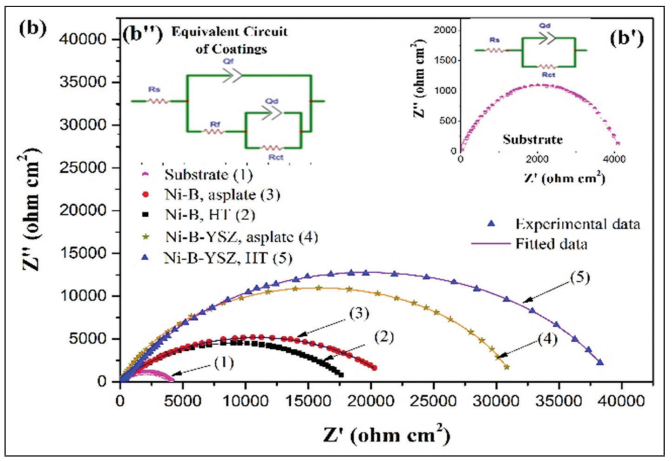
The Ni-B as-plated coating displays a lower corrosion current density (icorr) and a noble shift in corrosion potential (Ecorr) compared to the substrate, indicating improved protective ability. The cathodic overpotential reaction also shows a lower response, indicating a higher absorption of dissolved oxygen compared to the substrate. Additionally, the cathodic curve, except for the substrate, exhibits a similar reaction for coatings. The corrosion resistance of the heat-treated Ni-B coating is inferior to that of the Ni-B coating in its as-plated state. This is attributed to the presence of a non-homogeneous and amorphous structure in the as-plated coatings. The absence of a well-defined crystal structure in the as-plated state reduces the availability of sites for corrosion initiation, thereby improving the corrosion resistance of the coating [28].

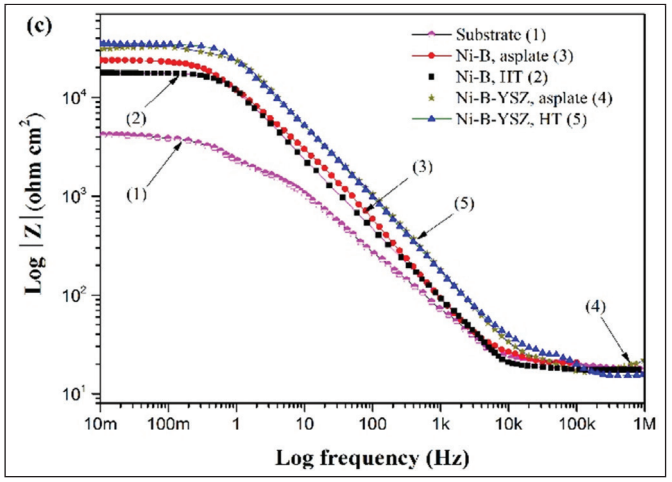
In the case of heat-treated nanocomposite coatings, exhibit relatively higher corrosion resistance. It exhibited the highest Rp value of ~ 36 kΩ-cm^2 (Table 2). This improvement in passivation behaviour can be attributed to several factors. Firstly, the heat treatment promotes the formation of a more protective and stable oxide layer on the coating surface, which acts as a barrier against corrosion. Secondly, the transformation to a more crystalline structure enhances the coating's overall corrosion resistance and passivation properties. Further, particle dispersion causes grain boundary obstruction, caused improved microstructure reduces the availability of corrosion pathways, hindering the diffusion of corrosive species and slowing down the corrosion process. Also, the interactions between the matrix and nanoparticles can create interfaces and boundaries that impede corrosion propagation, further enhancing the overall corrosion resistance [29,30].

On the other hand, in the as-plated state of nanocomposites, the corrosion processes may be accelerated due to the formation of micro-galvanic couplings between the matrix and particles. These micro-galvanic cells arise from the difference in electrochemical potentials between the dissimilar materials. As a result, an electrochemical reaction takes place, involving the transfer of electrons from the more active material (anode) to the less active material (cathode) within the galvanic cell. This electron transfer leads to the corrosion of the anodic material and the dissolution process during this anodic reaction [31].

The EIS technique was employed to obtain a Nyquist plot (Fig. 4b), which was then curve-fitted using an equivalent circuit. Figure 4b' represents the inset of substrate with equivalent circuit, while Fig. 4b'' represent the other coatings circuit. Rs denotes the resistance of the electrolyte solution, while Rct represents the charge transfer resistance. To account for the non-ideal behaviour of the double layer capacitance, a constant phase element, Qf, is employed. The double layer capacitance represents the charge transfer reaction occurring at the interface of coating and substrate called Qd.







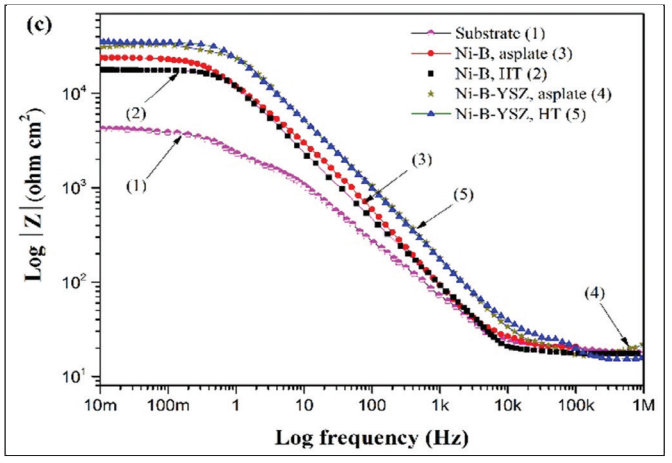


Fig. 4. Potentiodynamic polarization and EIS results for the substrate, Ni-B and Ni-B-YSZ (a) Tafel curve (b) Nyquist Curve (b') Nyquist Equivalent circuit for substrate and (b'') coatings (c) Bode impedance and (d) Bode phase angle plot.

The substrate exhibits a capacitance loop accordance to the charge transfer reaction, which can be assessed based on the diameter of the loop [26]. The enhanced resistance to corrosion of amorphous coatings can be attributed to lack of distinct crystallographic orientations or preferential pathways for corrosion propagation. Additionally, the amorphous coatings have higher chemical stability due to their disordered atomic arrangement, resulting in higher resistance than heat-treated ones [24]. Simultaneously, in other side, the charge transfer resistance (Rct) of the heat-treated Ni-B alloy coating is lower compared to that of the as-plated coating.

Table 2. The estimated corrosion parameters with use of potentiodynamic polarization curve.

Coating material	E_{corr} (V)	i_{corr} (μA/cm²)	β_a (mV/dec)	β_c (mV/dec)	R_p (kΩ-cm²)	Rct (kΩ-cm²)	CR (mm/yr)
Substrate	-0.56	22.0	134	708	2.23	4.18	0.507
Ni-B as plated	-0.46	0.92	134	100	27.06	23.88	0.019
Ni-B, HT	-0.51	1.18	134	146	25.66	17.83	0.025
Ni-B-YSZ as plated	-0.38	1.01	133	148	30.15	31.34	0.035
Ni-B-YSZ, HT	-0.36	0.65	128	95	36.47	35.19	0.022

The inclusion of nanocomposite coatings leads to an expansion of the Nyquist curve diameter, indicating an improvement in corrosion resistance. Specifically, in heat-treated conditions, the charge transfer resistance (Rct) of YSZ nano coatings is 35 kΩ.cm², which is notably higher than that of Ni-B/αZrP nano coatings (25 kΩ.cm²) [32]. Moreover, when compared to other nano coatings such as Ni-B-Al_2O_3 [21] and Ni-P-ZrO_2 [27], the value for YSZ nano coatings is approx. four and seven times higher, respectively. It should be noted that direct comparisons between these values are challenging due to variations in particle materials, matrix compositions, synthesis techniques for particle size and dispersion, and coating uniformity. Nevertheless, this demonstrates the better process control, ability of nanoparticle reinforcements to fill cracks and defects, resulting in enhanced corrosion resistance [31]. The as-plated Ni-B-YSZ shows slightly lower corrosion protection compared to the treated condition. This may be due to the porosity of the coating. These defects provide pathways for corrosive species to penetrate and attack the substrate. Additionally, the as-plated coating may have a less uniform and less dense microstructure

compared to the heat treated coating. This can result in the exposure of more active sites on the surface, increasing the likelihood of corrosion initiation and propagation.

A Bode plot is a valuable graphical tool that provides important insights into the frequency response of a system. It comprises of two plots: one illustrating the magnitude response and the other illustrating the phase response, as depicted in Fig. 4 (c and d). It is crucial to analyze the phase shift in conjunction with the corresponding magnitude response. The substrate exhibits unstable corrosion at lower frequencies, indicating lower resistance to corrosion. The as-plated coating of Ni-B alloy demonstrates a higher and stable magnitude, suggesting a significant resistance component associated with processes such as charge transfer resistance, diffusion, or ionic conduction. The heat-treated Ni-B coating shows lower impedance than as plated coating. In contrast, the heat-treated Ni-B-YSZ composite coating shows larger impedance than the as-plated coating. A higher magnitude in the impedance plot indicates a significant capacitive component, indicating the presence of a dielectric layer, oxide film, or double-layer capacitance at the electrode-electrolyte contact. The behaviour of impedance with respect to frequencies provides an indirect indication of the coating's low porosity, compact microstructure, columnar structure, chemical stability, and particle dispersion properties [33].

Further investigation of the Bode phase shift reveals similar resistance characteristics among the coatings. The existence of second-phase angle peaks found at the intersection of low frequencies in the Bode phase plot is recognised by experts as a sign of increased corrosion resistance [29]. The substrate demonstrates a bell-shaped curve indicating the continuous corrosion activity. The as-plated Ni-B coating shows a progressive shift, indicating the presence of a capacitive element at the contact area. The heat-treated Ni-B coating illustrates a shift towards higher frequencies, indicating a capacitive behaviour. The negative second phase shift observed at low frequencies in the nano-coatings indicates capacitive behavior associated with charge storage, often observed in passive or protective films on metal surfaces [34]. The similar second phase shift observed in the as-plated state of nanocomposite coatings suggests a comparatively reduced resistance to corrosion. The phase shift provides valuable insights into the favourable kinetics and reaction mechanisms involved in the corrosion process.

As a result, the as-plated Ni-B alloy coating demonstrated the lowest corrosion rate (CR) of approx. 0.019 mm/yr. (Table 2), while also having relatively low strength. Conversely, the treated Ni-B-YSZ coatings exhibited the highest strength with a comparable corrosion rate of 0.022 mm/yr.

4. Conclusions

In conclusion, an electroless nanocomposite coating was successfully applied by utilizing YSZ particles reinforced with a Ni-B matrix. This study's principal findings are summarised below:

a) Incorporating YSZ nanoparticles contributes to forming a more continuous and homogeneous Ni-B matrix, leading to a reduction in inherent defects in the coating.

b) Heat treatment enhances the mechanical characteristics of the coatings by promoting the formation of boride phases, including Ni_2B and Ni_3B, resulting in higher microhardness.

c) The corrosion resistance is deteriorated in heat treated condition than as-plated in case of Ni-B alloy coating.

d) In contrast, the corrosion resistance of Ni-B-YSZ coatings improves considerably with increased charge transfer resistance (~35 $K\Omega.cm^2$) under heat-treated conditions over as-plated states.

These findings emphasize the potential of electroless Ni-B-YSZ composite coatings for diverse applications, surpassing the performance of recent ceramic nano coatings.

References

[1] H. Li, G. Chen, K. Zhang, G. Luo, Z. Ye, Degradation failure features of chromium-plated gun barrels with a laser-discrete-quenched substrate, Surf. Coat Technol. 201 (2007) 9558–9564. https://doi.org/10.1016/j.surfcoat.2007.04.034.

[2] J.H. Underwood, G.N. Vigilante, C.P. Mulligan, Review of thermo-mechanical cracking and wear mechanisms in large caliber guns, Wear 263 (2007) 1616–1621. https://doi.org/10.1016/j.wear.2006.12.005.

[3] C.T. Dervos, J. Novakovic, P. Vassiliou, Vacuum heat treatment of electroless Ni-B coatings, Mater. Lett. 58 (2004) 619–623. https://doi.org/10.1016/S0167-577X(03)00581-0.

[4] B. Oraon, G. Majumdar, B. Ghosh, Improving hardness of electroless Ni-B coatings using optimized deposition conditions and annealing, Mater. Des. 29 (2008) 1412–1418. https://doi.org/10.1016/j.matdes.2007.09.005.

[5] S.K. Das, P. Sahoo, Study of potentiodynamic polarization behaviour of electroless ni-b coatings and optimization using Taguchi method and grey relational analysis, J. Miner. Mater. Charact. Eng. 10 (2011) 1307–1327. https://doi.org/10.4236/jmmce.2011.1014103.

[6] T.S.N.S. Narayanan, K. Krishnaveni, S.K. Seshadri, Electroless Ni-P/Ni-B duplex coatings: Preparation and evaluation of microhardness, wear and corrosion resistance, Mater. Chem. Phys. 82 (2003) 771–779. https://doi.org/10.1016/S0254-0584(03)00390-0.

[7] A. Mukhopadhyay, T.K. Barman, P. Sahoo, Tribological behavior of electroless Ni–B–W coating at room and elevated temperatures, Mater. Today Proc. 5 (2018) 3306–3315. https://doi.org/10.1016/j.matpr.2017.11.573.

[8] A. Mukhopadhyay, P. Sahoo, Effect of operating temperature on tribological behavior of as-plated Ni-B coating deposited by electroless method, Tribol. Trans. 61 (2018) 41–52.

[9] S. Duari, A. Mukhopadhyay, T.K. Barman, P. Sahoo, Optimization of wear performance of electroless Ni-B coating under lubrication, Int. J. Eng. Technol. 7 (2016) 94–103. https://doi.org/10.18052/www.scipress.com/ijet.7.94.

[10] A. standard B607-91(2003), Standard specification for autocatalytic nickel boron coatings for engineering use, ASTM Int. 02 (2009).

[11] D.E. and F. Bulbul, Preparation and characterization of electroless Ni–B/nano-SiO_2, $Al2O_3$, TiO_2 and CuO composite coatings, J. Sol-Gel Sci. Technol. 31 (2004) 83–86. https://doi.org/10.1023/B:JSST.0000047965.22232.53.

[12] S. Karthikeyan, L. Vijayaraghavan, S. Madhavan, A. Almeida, Study on the mechanical properties of heat-treated electroless NiP coatings reinforced with Al_2O_3 nano particles, Metall. Mater. Trans. A. 47 (2016) 2223–2231. https://doi.org/10.1007/s11661-016-3413-y.

[13] P. Sahoo, S.K. Das, Tribology of electroless nickel coatings - A review, Mater. Des. 32 (2011) 1760–1775. https://doi.org/10.1016/j.matdes.2010.11.013.

[14] A.E.-82(2003) Standard, Standard test method for Vickers hardness of metallic materials, ASTM Int. (n.d.).

[15] ASTM G5-14, Standard Reference test method for making potentiodynamic anodic polarization, Annu. B. ASTM Stand. (2014) 1–9. https://doi.org/10.1520/G0005-14.2.

[16] ASTM Norma G 106, Standard practice for verification of algorithm and equipment for electrochemical impedance measurements, ASTM 03 (1999) 1–11. https://doi.org/10.1520/G0106-89R10.2.

[17] K. Krishnaveni, T.S.N. Sankara Narayanan, S.K. Seshadri, Electroless Ni-B-Si_3N_4 composite coating: Deposition and evaluation of its characteristic properties, Synth. React. Inorganic, Met. Nano-Metal Chem. 42 (2012) 920–927. https://doi.org/10.1080/15533174.2011.618475.

[18] Y. Yang, W. Chen, C. Zhou, Fabrication and characterization of electroless Ni–P–ZrO_2 nano-composite coatings, Appl Nanosci. 1 (2011) 19–26. https://doi.org/10.1007/s13204-011-0003-6.

[19] M. Cecilia, C. De Sá, D. Moraes, C. Nelson, J. Duailibi, L. Guimarães, D. Oliveira, Mechanical properties of alumina-zirconia composites for ceramic abutments, Mater. Res. 7 (2004) 643–649.

[20] Z.A. Hamid, H.B. Hassan, A.M. Attyia, Influence of deposition temperature and heat treatment on the performance of electroless Ni-B films, Surf. Coat. Technol. 205 (2010) 2348–2354. https://doi.org/10.1016/j.surfcoat.2010.09.025.

[21] D. Mohanty, T.K. Barman, P. Sahoo, Characterisation and corrosion study of electroless Nickel-Boron coating reinforced with alumina nanoparticles, Mater. Today Proc. 19 (2019) 317–321. https://doi.org/10.1016/j.matpr.2019.07.216.

[22] Z.H. Huang, Y.J. Zhou, T.T. Nguyen, Study of nickel matrix composite coatings deposited from electroless plating bath loaded with TiB_2, ZrB_2 and TiC particles for improved wear and corrosion resistance, Surf. Coat. Technol. 364 (2019) 323–329. https://doi.org/10.1016/j.surfcoat.2019.01.060.

[23] Ş. Ürdem, E. Duru, H. Algül, M. Uysal, H. Akbulut, Evaluation of high temperature tribological behavior of electroless deposited NiB–Al_2O_3 coating, Wear (2021) 482–483. https://doi.org/10.1016/j.wear.2021.203960.

[24] K.N. Srinivasan, R. Meenakshi, A. Santhi, P.R. Thangavelu, S. John, Studies on development of electroless Ni-B bath for corrosion resistance and wear resistance applications, Surf. Eng. 26 (2010) 153–158. https://doi.org/10.1179/174329409X409468.

[25] V. Vitry, L. Bonin, Increase of boron content in electroless nickel-boron coating by modification of plating conditions, Surf. Coat. Technol. 311 (2017) 164–171. https://doi.org/10.1016/j.surfcoat.2017.01.009.

[26] A.F. Kanta, M. Poelman, V. Vitry, F. Delaunois, Nickel-boron electrochemical properties investigations, J. Alloys Compd. 505 (2010) 151–156. https://doi.org/10.1016/j.jallcom.2010.05.168.

[27] M.H. Sliem, K. Shahzad, V.N. Sivaprasad, R.A. Shakoor, Enhanced mechanical and corrosion protection properties of pulse electrodeposited NiP-ZrO_2 nanocomposite coatings, Surf. Coat. Technol. 403 (2020) 126340. https://doi.org/10.1016/j.surfcoat.2020.126340.

[28] A.F. Kanta, V. Vitry, F. Delaunois, Effect of thermochemical and heat treatments on electroless nickel–boron, J. Alloys Compd. 486 (2009) 21–23. https://doi.org/10.1016/j.jallcom.2009.07.038.

[29] Y.W. Song, D.Y. Shan, E.H. Han, Comparative study on corrosion protection properties of electroless Ni-P-ZrO_2 and Ni-P coatings on AZ91D magnesium alloy, Mater. Corros. (2007) 506–510. https://doi.org/10.1002/maco.200604033.

[30] M. Ghaderi, M. Rezagholizadeh, A. Heidary, S.M. Monirvaghefi, The effect of Al_2O_3 nanoparticles on tribological and corrosion behavior of electroless Ni–B–Al_2O_3 composite coating, Prot. Met. Phys. Chem. Surfaces,. 52 (2016) 854–858. https://doi.org/10.1134/S2070205116050087.

[31] Z. Wei, S. Hong, Z. Wei, N. Hu, G. Ying, Y. Wu, Comparison on long-term corrosion performance of WC-CoCr and Al_2O_3-TiO_2 ceramic coatings in sulphide-containing 3.5 wt% NaCl solution, Int. J. Refract. Met. Hard Mater. 107 (2022) 105906. https://doi.org/10.1016/j.ijrmhm.2022.105906.

[32] L. Yan, S. Yan, Y. He, Y. He, H. Li, R. Song, H. Zhou, X. Cheng, Preparation, corrosion resistance and mechanical properties of electroless Ni-B/α-ZrP composite coatings, Colloids Surf. A Physicochem. Eng. Asp. 654 (2022) 130132. https://doi.org/10.1016/j.colsurfa.2022.130132.

[33] T.S.N. Sankara Narayanan, S.K. Seshadri, Electro and electroless deposited composite coatings: Preparation, characteristics, and applications, Wiley Encycl. Compos. (2012) 1–17. https://doi.org/10.1002/9781118097298.weoc072.

[34] V. Niksefat, M. Ghorbani, Mechanical and electrochemical properties of ultrasonic-assisted electroless deposition of Ni-B-TiO_2 composite coatings, J. Alloys Compd. 633 (2015) 127–136. https://doi.org/10.1016/j.jallcom.2015.01.250.